Systematic exploration into the hemodynamic effect of an out-of-plane internal carotid artery

This article may be found at
http://www.soton.ac.uk/~cedc/posters.html

Neil W. Bressloff [1], Jim Banks [1], Cliff P. Shearman [2]

[1] Computational Engineering and Design Group
School of Engineering Sciences
University of Southampton
Southampton, UK

[2] Department of Vascular Surgery
Southampton General Hospital
Southampton, UK

Introduction

This article presents a systematic exploration of the effect that an out-of-plane internal carotid artery (ICA) has on the shear stress in the human carotid artery bifurcation. Starting from a mean, planar bifurcation geometry based on the data in [1] and defined in CATIA V5 (Dassault Systemes), the ICA is parameterised such that its shape can be automatically manipulated out-of-plane. The external carotid artery (ECA) and the common carotid artery (CCA) are maintained in fixed planar positions.

Interest in the impact of arterial non-planarity has increased in recent years, largely driven by an incomplete understanding of the risk factors for atherogenesis [2] and by the desire to improve the failure rates associated with bypass grafts [3]. There are a limited number of earlier studies that investigate the effects of three-dimensional vascular geometries [4].

Here, we seek to complement this growing body of work by constructing a landscape that describes how the area-weighted integral of negative time-averaged shear stress (AWINTASS) [5] varies with the out-of-plane position of the ICA. AWINTASS is defined as

$$\bar{\bar{\tau}} = \int |\bar{\tau}_-| dA_- / \int dA_-$$

where, respectively, $\bar{\tau}_-$ and dA_- denote time-averaged shear stress and surface area on boundary elements for which $\bar{\tau} < 0$.

Geometry Exploration

Parametric CAD models facilitate systematic variation of specific geometric parameters such that individual geometries can be automatically constructed and meshed in preparation for analysis. When embedded in a design search and optimization loop the computational expense of unsteady, three-dimensional computational fluid dynamics (CFD) simulation predicates against the use of direct search methods. Instead, a surrogate model is typically constructed using a response surface methodology [6]. This is depicted in Figure 1. Having constructed the parametric geometry model, and established a process for mesh construction and CFD simulation - a typical geometry is shown in Figure 2 - it is necessary to first populate the design space of all feasible designs (or geometries) using a design of experiments (DoE). Meshes are constructed and CFD simulations are performed for all geometries. In order to compare the performance of individual geometries, an output metric (or objective function) is required for each. A single metric is used here, AWINTASS. A similar metric is shown to provide an effective measure of regions of reverse flow in [5]. Other metrics that could have been used include those recently discussed by Hyun et al [7]. A surface is fitted to this vector of objective function values using the method of kriging [8] which readily provides a measure of uncertainty that can be used to identify where update points should be sampled to improve the quality of the fit and efficiently seek the global optimum. Typically, new krigs are constructed following both the initial DoE and each set of updates. When constructing the krig (either from the initial DoE or from the DoE and the update points) a tuning process is performed that seeks to maximize the log-likelihood function [8].

The out-of-plane location of the ICA is defined by polar co-ordinates relative to its mean position (in-plane with the ICA and CCA and centred 20mm from the centre of the ECA). The exploration space is defined by radii and angles varying between 0 and 30mm, and 0 and 165 degrees, respectively. In the results presented below, both measurements are non-dimensionalised between 0 and 1.

CFD Setup

Unsteady flow simulations are performed using FLUENT (Fluent Inc.) employing the PISO numerical scheme, and second order accuracy in space and time. Blood is treated as a Newtonian fluid. The mass fluxes through the ICA and ECA branches are set in the ratio 70:30. A mean pulse is employed [5] with a time step of 10^{-5}s. A hybrid hex-core mesh is generated in GAMBIT (Fluent Inc.) with a fixed mesh interval size of 0.96mm.

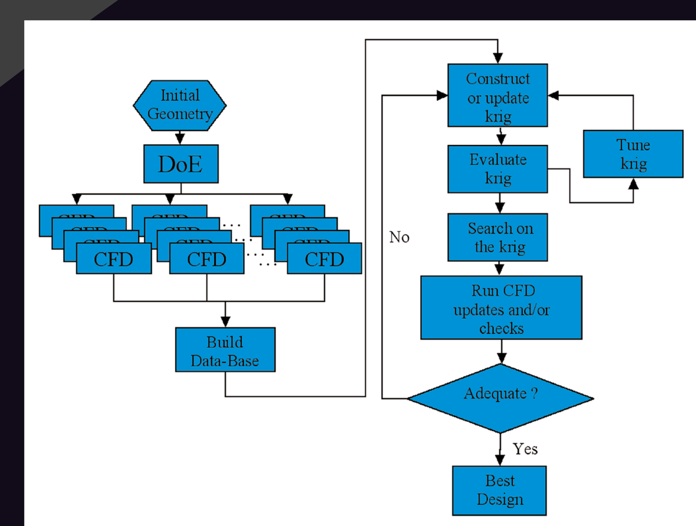

Figure 1 Response surface methodology.

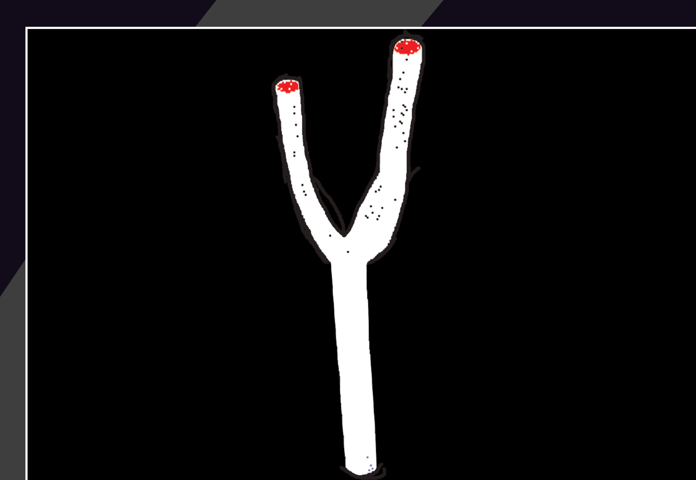

Figure 2 Example geometry.

Results and Discussion

Limitations of space preclude presentation of the initial response surface, so Figure 3 depicts a regressed response surface for the DoE (plus symbol) and the first set of update points (asterix symbol), comprising the predicted maximum and minimum of the initial response surface together with four points located at the positions of largest error. A second, similar set of update points (circle symbol) produce the response surface shown in Figure 4.

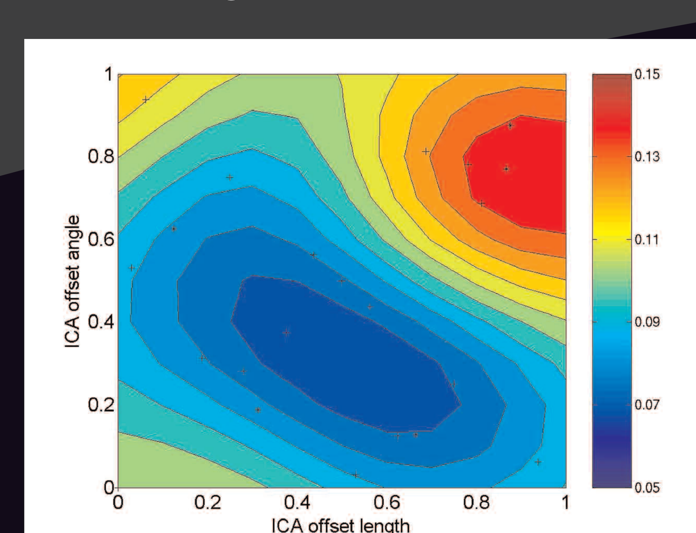

Figure 3. Response surface for AWINTASS (Pa) after the first set of updates.

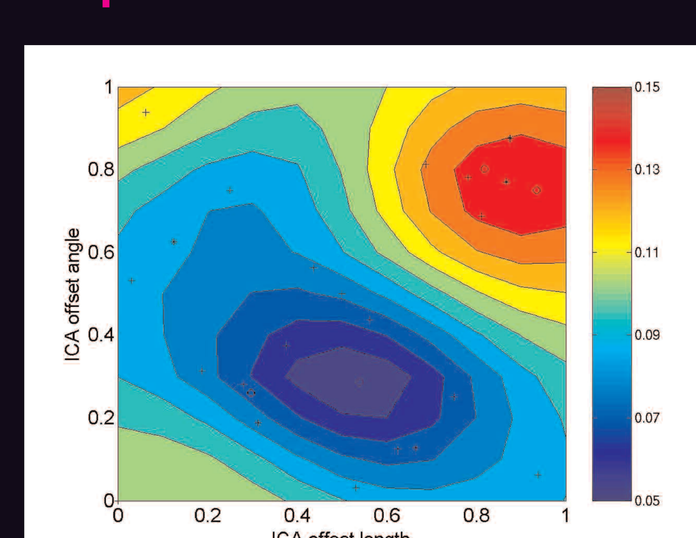

Figure 4. Response surface for AWINTASS (Pascals) after the second set of updates.

Although the response surface in Figure 4 is not fully converged, it is clearly converging with a distinct maximum (0.1456Pa at 26.96mm, 126.67 degrees) and minimum (0.0516Pa at 15.73mm, 47.32 degrees). The reasons for the locations of these turning points are not clear. However, inspection of the flow during and after the strong deceleration phase of systole suggests that greater swirling produced by geometries that are further out-of-plane (towards the top right corner of Figure 4) leads to stronger re-circulation in the sinus bulb, and, hence, larger values of AWINTASS. The geometry producing the maximum value of AWINTASS is depicted in Figure 5: a plan view is shown along with a set of two-dimensional slices (downstream from the bifurcation) and the associated regions of reversed flow half way through the pulse. Figure 6 shows similar features for the geometry that generates the minimum value of AWINTASS; here, the regions of reversed flow are significantly weaker and further from the wall.

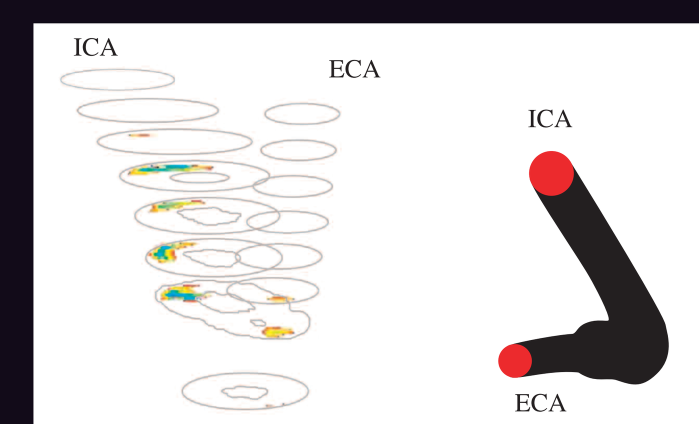

Figure 5. Geometry producing maximum AWINTASS

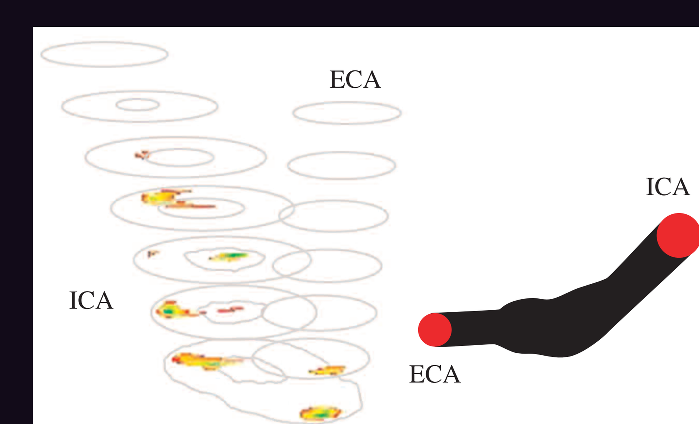

Figure 6. Geometry producing minimum AWINTASS

References

1. Ding, Z., Wang, K., Li, J. and Cong, X., 2001. "Flow Field and Oscillatory Shear Stress in a Tuning-Fork-Shaped Model of the Average Human Carotid Bifurcation," J. Biomech. Eng., Vol. 34, pp. 1555-1562.

2. Thomas, J. B., Milner, J. S., and Steinman, D. A., 2002, "On the Influence of Vessel Planarity on Local Hemodynamics at the Human Carotid Bifurcation", Biorheology, Vol. 39, Nos. 3-4, pp. 443-448.

3. Papaharilaou, Y., Doorly, D. J., and Sherwin, S. J., 2002, "The Influence of Out-of-Plane Geometry on Pulsatile Flow within a Distal End-to-Side Anastomosis", J. Biomech., Vol. 35, pp. 1225-1239.

4. Caro, C. G., Doorly, D. J., Tarnawsk, M., Scott, K. T., Long, Q., and Dumoulin, C. L., 1996, "Non-Planar Curvature and Branching of Arteries and Non-Planar Type Flow", Proc. Roy. Soc. Lon. A, Vol. 452, pp. 185-197.

5. Bressloff, N. W., Banks, J., and Bhaskar, K. V., 2004, "Parametric Geometry Modeling of the Carotid Artery Bifurcation; the Need for New Flow Metrics", Proceedings, 2004 Workshop on Flow and Motion, Zurich, Switzerland, pp. 104-105.

6. Forrester, A. I. J., Bressloff, N. W., and Keane, A. J., 2003, "Response Surface Model Evolution," 16th AIAA Computational Fluid Dynamics Conference, AIAA-2003-4089, Orlando, USA.

7. Hyun, S., Kleinstreuer, C., Longest, P. W., and Chen, C., 2004, "Particle-Hemodynamics Simulations and Design Options for Surgical Reconstruction of Diseased Carotid Artery Bifurcations", J. Biomech. Eng., Vol. 126, pp. 188-195.

8. Jones, D. R., Schlonlau, M. and Welch, W. J., 1998, "Efficient Global Optimisation of Expensive Black-Box Functions" J. Glob. Opt., 13, 455-492.

Contact:
N.W.Bressloff@soton.ac.uk

University of Southampton